Metallic porous electrodes enable efficient bicarbonate electrolysis

Zishuai Zhang,[1] Faezeh Habibzadeh,[1] Danielle A. Salvatore,[2] Shaoxuan Ren,[1] Eric W. Lees,[2] and Curtis P. Berlinguette*[1,2,3,4]

[1]Department of Chemistry, The University of British Columbia, 2036 Main Mall, Vancouver, British Columbia, V6T 1Z1, Canada.

[2]Department of Chemical and Biological Engineering, The University of British Columbia, 2360 East Mall, Vancouver, British Columbia, V6T 1Z3, Canada.

[3]Stewart Blusson Quantum Matter Institute, The University of British Columbia, 2355 East Mall, Vancouver, British Columbia, V6T 1Z4, Canada.

[4]Canadian Institute for Advanced Research (CIFAR), 661 University Avenue, Toronto, M5G 1M1, Ontario, Canada.

*Corresponding author: Curtis P. Berlinguette (cberling@chem.ubc.ca)

Highlights:

- The electrolysis of bicarbonate solutions presents the opportunity to utilize liquid feedstocks that are easier to engineer than systems that require gaseous CO_2
- Porous silver foam electrodes enables the electrolysis of bicarbonate solutions at rates commensurate with gaseous CO_2 feedstocks
- The efficient electrolysis of bicarbonate provides a viable path for converting air capture solutions into useful products without the need for costly separations and pressurization steps

Context & Scale

Developing technologies to store intermittent wind and solar energy is a key step towards decarbonizing the global economy. The CO_2 reduction reaction (CO_2RR) is a promising strategy that enables renewable energy to be stored in chemicals and fuels using atmospheric or emitted CO_2. Pilot-scale electrolyzers that use a gaseous CO_2 feedstock (instead of CO_2 dissolved in water) can mediate high rates of CO_2RR, but this approach is challenged by the energy-intensive processes required to produce purified, high pressure CO_2 from carbon capture.

We show in this work the electrochemical conversion of carbon capture solutions (i.e., bicarbonate) directly into chemical building blocks (i.e., CO + H_2) using highly-active and robust metallic electrodes. This study demonstrates bicarbonate electrolysis as a practical strategy for storing renewable energy in carbon chemicals while bypassing CO_2 separation and pressurization processes in upstream CO_2 capture. capture.

Summary

We demonstrate here that a porous free-standing silver foam cathode in an electrolytic flow cell mediates efficient electrolysis of 3.0 M bicarbonate solutions into CO. These results have direct implications for carbon capture schemes where OH^- solutions react with CO_2 to form bicarbonate-rich solutions that need to be treated to recycle the sorbent and recover the CO_2. Our study shows a viable path for replacing the high-temperature thermal process currently used to recover CO_2 from these carbon capture solutions by using electricity to drive the conversion of bicarbonate into CO_2 and subsequently into CO. The use of free-standing porous silver electrodes was found to yield electrolysis performance parameters (e.g., a Faradaic efficiency for CO production, FE_{CO}, of 78% at 100 mA cm^2; <3% performance loss after 80 h operation) that are superior to results obtained in bicarbonate electrolyzers that utilize conventional carbon-based gas diffusion electrodes (GDEs) designed for gaseous CO_2 fed electrolyzers. These performance metrics are comparable to any electrolytic flow cell fed directly with a CO_2 feedstock, with the added benefit of not requiring an energy-intensive pressurization step that would be necessary for the electrolysis of gaseous CO_2. These findings represent a potentially important step in closing the carbon cycle.

Keywords

Bicarbonate electrolysis; CO_2 reduction reaction; flow cell; silver foam; gas diffusion electrode.

Table of contents graphic

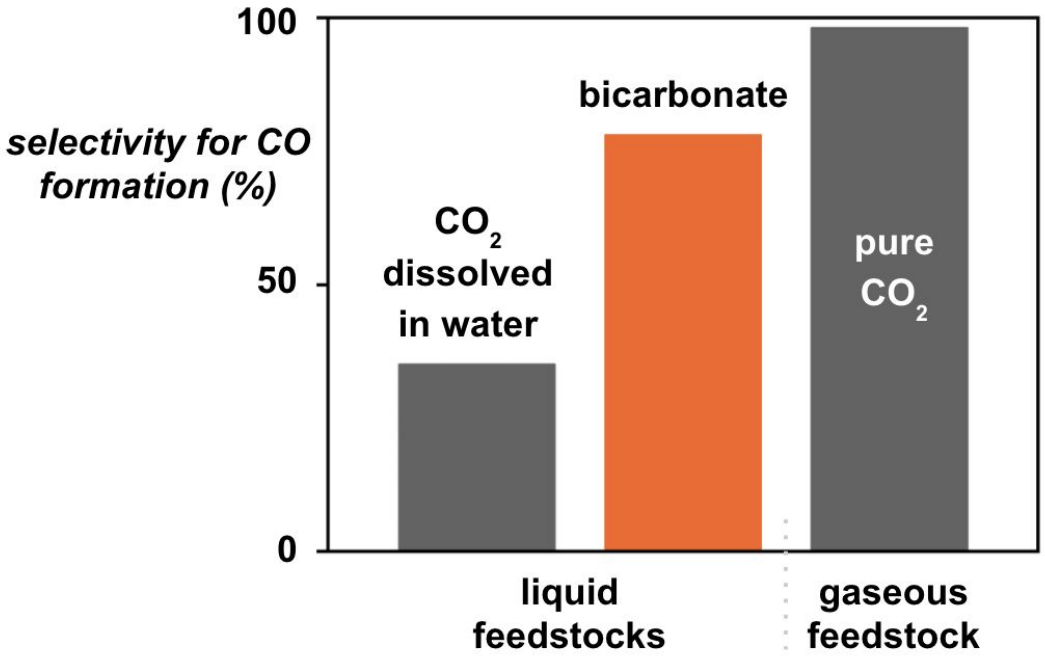

Introduction

In order to utilize CO_2 captured from the atmosphere or a point source, the captured CO_2 needs to be extracted from the sorbent in such a way that the sorbent can be recycled to capture additional CO_2. Schemes that rely on basic solutions such as KOH to capture CO_2 by forming carbonate (Eqs. 1 and 2) use a high temperature calcination step (> 900 °C) to subsequently liberate CO_2 (which can then be stored or utilized) from the carbonate salt with the concomitant recovery of the OH^- sorbent (Eqs. 3 and 4, Figure 1).[1] This recovery process involving the thermal decomposition of $CaCO_3$ at 900 °C is expensive because it uses two preheat cyclones along with a calciner in succession that are both energy and capital intensive.[1] One promising option for using this CO_2 is to electrolytically convert it into chemicals or fuels of economic value (e.g., CO) using renewable electricity (Eq. 5, Figure 1).[2,3] While there have been many recent advances in electrolytic CO_2 reduction,[2,4–7] the electrolysis of CO_2 will likely require an energy-intensive CO_2 pressurization step prior to electrolysis in order to achieve meaningful reaction rates (Figure 1).[8]

CO_2 capture:	$CO_{2\,(g)} + 2\ KOH_{(aq)} \rightleftharpoons K_2CO_{3\,(aq)} + H_2O_{\,(l)}$, ($pK_b$ 3.7)	Eq.1
KOH regeneration:	$K_2CO_{3(aq)} + Ca(OH)_{2\,(s)} \rightleftharpoons CaCO_{3\,(s)} + 2\ KOH_{(aq)}$	Eq.2
CO_2 recovery:	$CaCO_{3\,(s)} \rightleftharpoons CO_{2\,(g)} + CaO_{\,(s)}$	Eq.3
Sorbent regeneration:	$CaO_{\,(s)} + H_2O_{\,(l)} \rightleftharpoons Ca(OH)_{2\,(s)}$	Eq.4
CO_2 reduction reaction (CO_2RR):	$CO_{2\,(g)} + H_2O_{(l)} + 2e^- \rightleftharpoons CO_{(g)} + 2OH^-_{(aq)}$	Eq.5

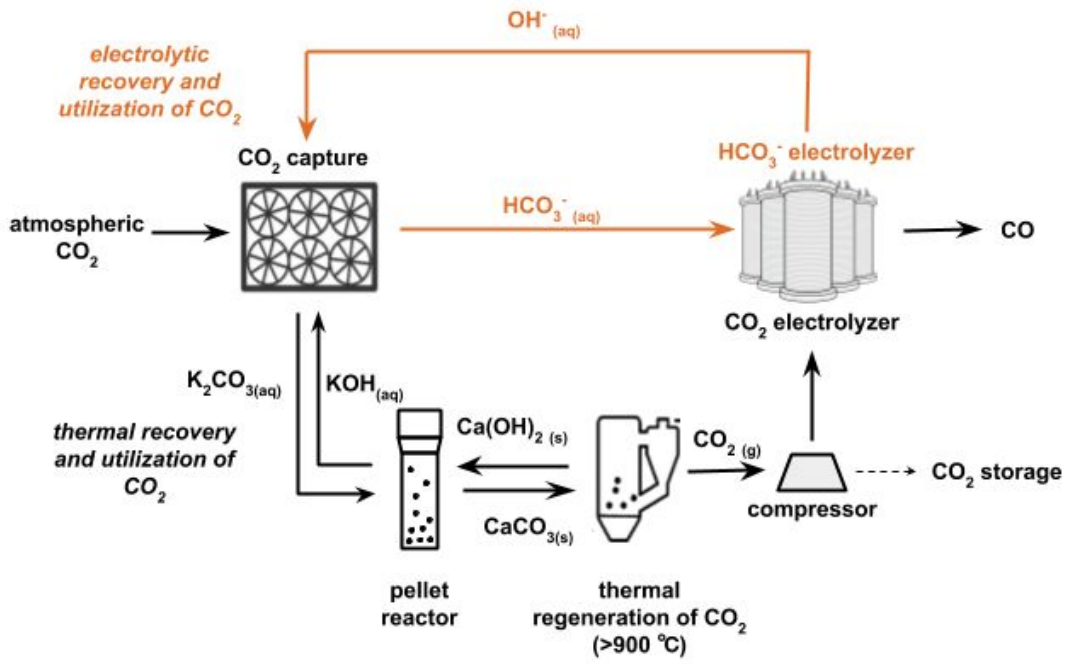

Figure 1. **Thermal CO_2 and sorbent recovery (black) and electrolytic recovery of CO_2 (orange) processes to convert captured atmospheric CO_2 to CO.** For the direct air capture process, atmospheric $CO_{2(g)}$ is captured by hydroxide solutions and then regenerated from $CaCO_{3(s)}$ in a high temperature calcination step (>900 °C). The recovered CO_2 typically needs to be pressurized prior to electrolysis or storage (black). For the bicarbonate electrolysis process, carbon capture solution (HCO_3^-) is electrochemically converted to CO without the need for energy intensive calcination and pressurization steps (orange). The hydroxide byproduct can be recycled for use as a carbon capture solution in the bicarbonate electrolysis pathway.

Our program is therefore seeking methods that avoid the calcination and pressurizations steps by developing reactor architectures that utilize bicarbonate solutions obtained during the CO_2 capture process as the cathodic feedstock while regenerating the OH^- sorbent for subsequent carbon capture (Figure 1, orange loop).[1,9–12] This proposed carbon capture and utilization scheme links CO_2 electrochemistry with upstream carbon capture without requiring high temperature or pressurization processes. A major technical challenge associated with this scheme is that bicarbonate cannot be directly electrochemically reduced. Bicarbonate must first react with protons to form CO_2, which is the

electrocatalytically active species that can be reduced to CO or other carbon-containing products. The management of this acid-base chemistry (Eq. 6) in tandem with electrochemistry (Eq. 5) therefore requires the careful design of an electrolyzer before liquid bicarbonate feedstocks can be deemed suitable for electrolysis. It is for these reasons that we are seeking ways to have protons delivered from a membrane, such as a bipolar membrane (BPM), for reaction with bicarbonate to form electrocatalytically active CO_2 at the membrane-catalyst interface.[11,13]

Conversion of bicarbonate: $H^+_{(aq)} + HCO_3^-{}_{(aq)} \rightleftharpoons H_2O_{(l)} + CO_{2\,(g)}$ Eq.6

For electrolyzers that use a gaseous CO_2 feedstock, gas diffusion electrodes (GDEs) are designed to support an electrocatalyst layer while also managing the water content at the cathodic side of the membrane electrode assembly (MEA). Flooding of the MEA with water needs to be avoided because it decreases the performance of electrolyzers by hindering CO_2 access to the catalyst layer. Excess water also promotes the undesirable hydrogen evolution reaction (HER) to occur over the CO_2 reduction reaction (CO_2RR).[14] GDEs used for electrolysis of gaseous CO_2 typically consist of a three-layer structure containing: (i) a conductive, porous carbon cloth positioned against the cathodic flow plate; (ii) a conductive and hydrophobic microporous layer (MPL) of carbon black treated with polytetrafluoroethylene (PTFE); and (iii) a catalyst layer between the MPL and the membrane (Figure 2a). The hydrophobicity of the MPL serves to mitigate flooding, and the mitigated flooding helps reduce ohmic losses and increases the accessible active area of the catalyst layer.[15]

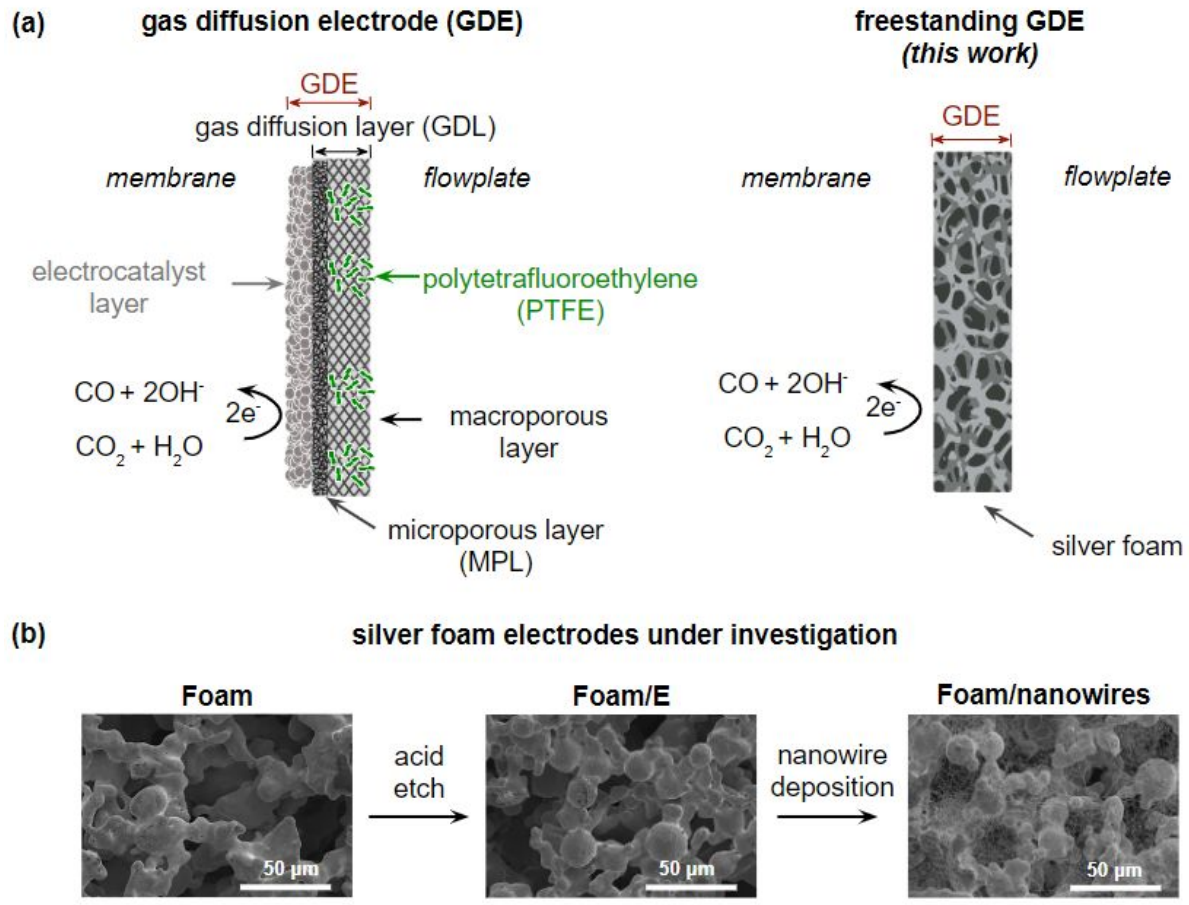

Figure 2. **Schematics of a conventional GDE and a free-standing silver foam GDE.** (a) Schematic depictions of the conventional GDE cathode with a microporous layer (MPL) and polytetrafluoroethylene (PTFE) treatment, and the free-standing silver foam GDE. Bicarbonate ions are the reactants for *in-situ* CO_2 generation at the membrane-catalyst interface, and the produced CO_2 is subsequently reduced to CO (see Eqs. 5 and 6). (b) SEM images of the **Foam, Foam/E** and the **Foam/nanowires** GDEs under investigation.

While these GDE designs are effective for the electrolysis of *gaseous* CO_2, they are not necessarily effective for the electrolysis of *liquid* feedstocks such as bicarbonate. Consider that commercial liquid-fed electrolyzer systems (e.g., water electrolyzers and chlor-alkali electrolyzers),[16,17] use free-standing electrodes and not GDEs as described above. Free-standing porous nickel (alloys), or steel electrodes coated with nickel, are capable of operating at lower overpotentials with longer lifetimes relative to GDEs in alkaline water electrolyzers.[18,19] Commercial chlor-alkali electrolyzers also use

titanium-based and nickel-based free-standing electrodes.[17,20,21] Moreover, hydrophobic GDEs inhibit the transport of solvated HCO_3^-, therefore adversely affecting the *in-situ* CO_2 generation (*i*-CO_2) at the membrane-GDE interface.[22] Replacing hydrophobic GDEs with metallic porous electrodes is anticipated to facilitate the transport of solvated ions and improve the performance of the bicarbonate electrolyzer.[23]

These collective observations inspired us to test porous free-standing silver foam electrodes for liquid bicarbonate fed electrolysis. Not only these free-standing electrodes simplify the assembly of flow cells relative to conventional GDEs (which require a multi-step fabrication process), these metallic electrodes mediate remarkably effective bicarbonate electrolysis (e.g., a faradaic efficiency for CO production (FE_{CO}) of 72 ± 3% at 100 mA cm^{-2} at 20 °C) and incur a merely 3% loss in FE_{CO} over 80 h of sustained electrolysis at 65 mA cm^{-2}. These results are superior to that of our control experiments with conventional GDEs (i.e., multilayer structure of a catalyst layer adjacent to a hydrophobic GDL as a support) which yielded peak FE_{CO} values of 33 ± 6% and suffered from 15% loss in FE_{CO} during our 80 h stability test. We achieved these results with the metallic electrodes by acid-etching and coating the surfaces with silver nanowires to generate higher catalytic activity. We also found that increasing the temperature of the bicarbonate feedstock, and the dynamic equilibria of the solution, suppresses HER and leads to higher FE_{CO} values. The bicarbonate electrolyzers reported herein demonstrate comparable performance to state-of-the-art gaseous CO_2 fed electrolyzers (Figure 3, Table S2), providing an opportunity to close the current upstream carbon capture loop and avoid the costly calcination and pressurization steps.

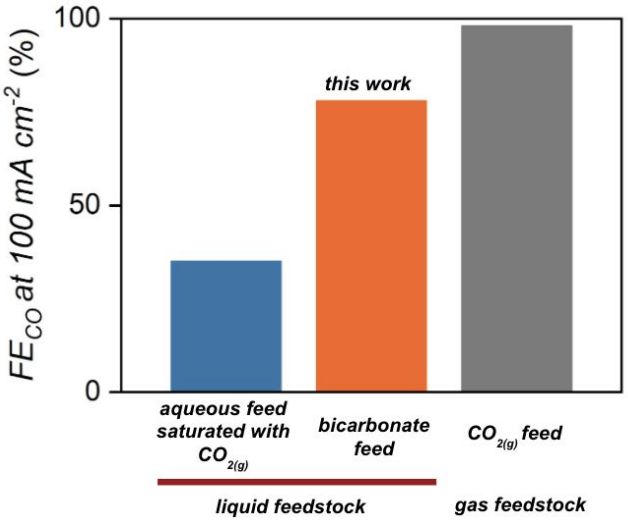

Figure 3. State-of-the-art FE_{CO} values for zero-gap electrolyzers designed to reduce CO_2 using three different feedstocks: aqueous feedstocks saturated with CO_2 (blue), bicarbonate feedstocks (orange), and gaseous CO_2 (grey).[11,24–30] See Table S2 for additional details.

Results and Discussion

All electrolysis experiments were conducted in a two-electrode MEA flow cell (Figure S1).[11,25] The MEA consisted of a fully hydrated Fumasep bipolar membrane (BPM) sandwiched between the anode (Ni foam) and the cathode (conventional GDEs or silver foam-based electrodes). The BPM was operated in reverse-bias mode, with the cation exchange layer facing the cathode.[13] A peristaltic pump delivered 1.0 M KOH to the anode at a constant flow rate of 40 ml min^{-1}. The 3.0 M $KHCO_3$ cathode electrolyte was delivered separately at a constant flow rate of 50 ml min^{-1}. The headspace of the cathode electrolyte reservoir was purged with N_2 at 160 sccm over the course of each experiment. Product gases and N_2 in the headspace of the cathode electrolyte reservoir were delivered to an in-line gas chromatograph (GC) with data analysis and peak integration completed in PeakSimple software. The temperature of the catholyte reservoir was controlled with a water bath set to 20, 40, 60, or 80 °C. The flow cell inlet temperatures were measured using in-line resistance temperature detectors (RTDs).

The bicarbonate electrolysis experiments were designed to test modifications of the cathodes: silver foam (denoted as "**Foam**"); etched silver foam (denoted as "**Foam/E**"); and etched silver foam coated with silver nanowires (denoted as "**Foam/nanowires**") (Figure 2b). Silver was selected as the cathode of choice because it mediates effective conversion of CO_2 to CO.[31,32] The **Foam** samples (2 cm × 2 cm × 200 μm) were prepared by washing commercially available silver foams with deionized (DI) water and isopropanol (IPA). The **Foam/E** electrodes were prepared by etching **Foam** in dilute nitric acid (30% v/v HNO_3) for 10 seconds (Figure 2b), where the **Foam/nanowires** electrodes were prepared by airbrushing an ink composed of 200 μL silver nanowires solution (dispersed in 2 ml of isopropyl alcohol) onto each side of the **Foam/E** electrode (Figure 2b).

Scanning electron microscopy (SEM) imaging of the porous **Foam** showed the silver foam skeletal structure consists of a smooth surface with few cracks and holes (Figure 2b). The etched surface of **Foam/E** contains a high number of cracks and holes (Figures 2b, S2). The silver nanowires with diameters of ~70 nm were immobilized on the walls of the pores of the silver foam for the **Foam/nanowires** electrode (Figures 2b, S3, S4). The nanowires were observed from the surface to a depth of 60-100 μm on each side of the foam (Figure S4). The X-ray diffraction (XRD) measurements of each electrode indicated signals at 38°, 44° and 64° corresponding to metallic silver (111), (200) and (220) facets, respectively (Figure S5). These signals are consistent with metallic silver (Ag^0) being the main constituent of the samples. The electrochemical surface areas (ECSA) of the silver electrocatalyst in the **Foam**, **Foam/E**, **Foam/nanowires** and **GDE/control**, estimated from the double-layer capacitance (C_{dl}) measurements (Figure S6), were significantly higher than that of the **GDE/control**. Etching the **Foam** to form **Foam/E** increased the ECSA by ~1.2-fold, while the addition of the nanowires to form **Foam/nanowires** exhibited a 2.6-fold increase in ECSA. Beyond changes in ECSAs, the intrinsic activity of the acid-etched **Foam/E** may also be higher than the **Foam** because of the rougher curved surfaces, which have been claimed to stabilize CO_2^- intermediates (i.e., a higher

roughness factor; roughness factor = ECSA / geometric electrode area).[33] Further modification with nanowires enhances the activity by increasing the abundance of exposed corner and edge active sites that promote chemisorption of both reactants and key intermediates.[34,35] Additionally, The high length-to-diameter ratio afforded by nanowire decoration, provided excess pores and channels for the transport of CO_2 and electrolyte that would result in a faster reaction rate.[36]

The three different silver foam electrodes were tested in a flow cell under constant applied current densities of 100, 200 and 300 mA cm^{-2}. Control experiments were performed with a CeTech® woven carbon cloth support containing a layer of silver nanoparticles (denoted as "**GDE/control**"). The **GDE/control** contains an MPL and PTFE common to gas-fed electrolyzers.[37,38] Electrolysis experiments using **GDE/control** at an applied current density of 100 mA cm^{-2} for 500 seconds yielded a FE_{CO} value of 33 ± 6%. This benchmark was exceeded by the **Foam**, which achieved a FE_{CO} value of 52 ± 2%. This difference in FE_{CO} was maintained over a 100-300 mA cm^{-2} range (Figure 4a). At 100 mA cm^{-2}, the cell voltage (V_{cell}) of the **Foam (**3.7 ± 0.1 V) was slightly higher than that of **GDE/control** (3.4 ± 0.1 V, Figure S7). The higher cell voltages obtained with the foam electrodes relative to the **GDE/control** electrodes comes despite porous metals being two orders-of-magnitude more conductive than carbon GDLs (i.e., ~10^5.S m^{-1} [39] *c.f.* ~10^3 S m^{-1})[40]. This difference in cell potentials may therefore be related to a relatively higher tortuosity compared to GDE/control electrodes, the foams retain larger volumes of the electrolyte which consequently introduces a greater solution resistance. Moreover, the contact resistances between the MPL and the membrane is lower.[41] These factors are difficult to experimentally resolve in a dynamic flow cell environment. Nevertheless, there are several properties of silver foam electrodes that can be tuned to reduce voltage losses: thickness, pore size distribution, surface roughness, etc.

The FE_{CO} was further increased by the higher ECSA **Foam/E** to 59 ± 6% at 100 mA cm^{-2} while maintaining a similar V_{cell} (3.6 ± 0.1 V) to **Foam**. We operated a flow cell at 100 mA cm^{-2} for 1 h and tracked the amount of CO and CO_2 exiting the flow cell by GC. Experiments with **Foam/E** and **GDE/control** showed similar amounts of CO_2 exiting the flow cell, but **Foam/E** generated a higher amount of [*i*-CO_2] relative to the **GDE/control**, and also produced a lower $[CO_2]_{outlet}$ to [*i*-CO_2] ratio (Figure S8). The addition of the silver nanowires to the **Foam/E** increased FE_{CO} to 72 ± 3% at 100 mA cm^{-2} (3.7 ± 0.1 V; Figure 4a). At 300 mA cm^{-2}, the **Foam/nanowires** yielded a FE_{CO} of 34% at 300 mA cm^{-2}, corresponding to a H_2:CO ratio (~2) relevant to downstream chemical production.[42] Note that we measured liquid product formation for all the preceding experiments using ^{1}H NMR spectroscopy, and determined that all $FE_{formate}$ values were <1% (Figure S9).

We observed that the efficiency of bicarbonate electrolysis could be improved by increasing the temperature of the electrolyte to 70 °C (Figure 4a). Using the **Foam/E** electrodes, an electrolyte temperature at the flow cell inlet of 70 °C yielded a FE_{CO} of 78 ± 4% at 100 mA cm^{-2} with a corresponding voltage of 3.5 ± 0.1 V (*c.f.* FE_{CO} of 59 ± 6% at 20 °C). Temperature can improve electrolyzer performance (i.e., improved FE_{CO}) in a number of ways. For example, higher temperatures lower CO_2 solubility, thereby extracting more CO_2 from the bicarbonate solution.[43] Higher temperatures would also increase CO_2 generation by increasing the bicarbonate dissociation kinetics (Eq. 7),[44] and also shifts the equilibrium towards CO_2 (Eq. 6, ΔH = 11.77 kJ mol^{-1}; Figure S10). These reactions also increase the pH, thereby suppressing HER (Figure S11). This observation is supported by the GC measurements. Higher temperatures would yield faster mass transfer kinetics for HCO_3^- and CO_2, which would also be expected to enhance the rate of bicarbonate electrolysis.[45]

Bicarbonate dissociate: $HCO_3^- \leftrightharpoons OH^- + CO_2$ Eq.7

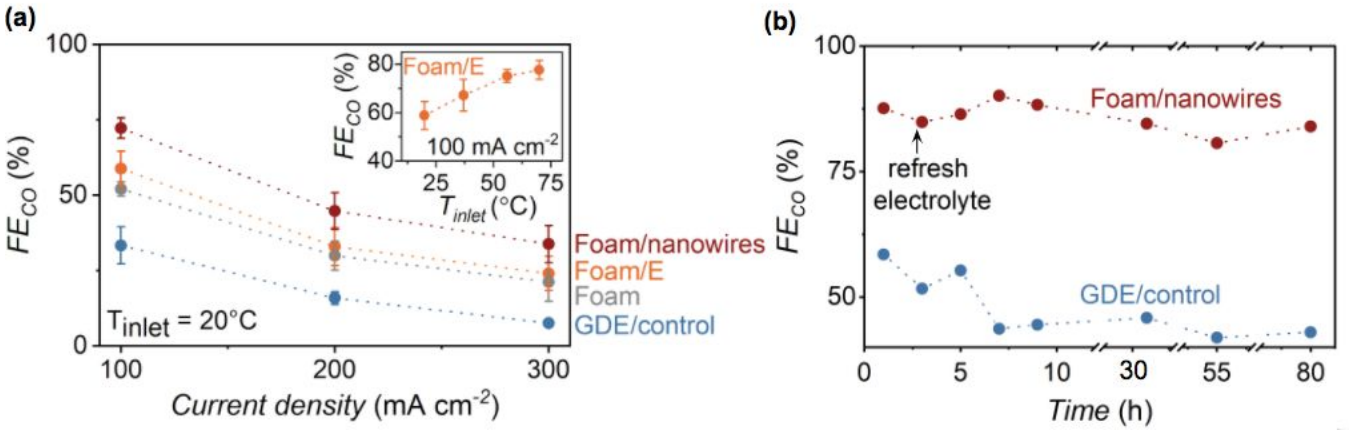

Figure 4. **Catalytic performance of the free-standing foam electrodes and conventional GDEs**. (a) FE_{CO} as a function of current density for the four cathodic GDEs (geometrical surface area = 4 cm^2; T_{inlet} = 20 °C). Inset: FE_{CO} values as a function of inlet temperature (T_{inlet} = 20, 37, 56 and 70 °C) at 100 mA cm^{-2}. T_{inlet} is the temperature of the bicarbonate solution entering the cathodic flowplate. The uncertainty is the standard deviation of 3 independent measurements. (b) FE_{CO} at a constant applied current density of 65 mA cm^{-2} (T_{inlet} = 20 °C) for 80 h for the **Foam/nanowires** and the **GDE/control** electrodes.

Stability studies were performed by electrolysing 3.0 M bicarbonate over 80 hours at an applied current density of 65 mA cm^{-2} using a flow cell containing **Foam/nanowires** or **GDE/control** (Figure 4b). (We used 65 mA cm^{-2} instead of 100 mA cm^{-2} to reduce the rate at which the bicarbonate reagent concentration decreased with time.) Bicarbonate concentrations were held constant by manually refreshing the 3.0 M $KHCO_3$ electrolyte 500 seconds before each GC measurement. Unlike the catholyte solution, the KOH anolyte solution was not refreshed, since the continuous supply of OH^- from the anion exchange side of the BPM is expected to maintain the pH of the anolyte. The FE_{CO} decreased by merely 3% over this 80 h period for **Foam/nanowires**. Notably, the **GDE/control** exhibited a much larger decrease of 16% over the same time period. SEM imaging of **Foam/nanowires** showed that the

silver nanowires on the top of the silver foam surface remained intact (Figure S12), while the morphology of the silver nanoparticle catalyst layer in **GDE/control** electrode underwent much more dramatic morphological changes to yield a smoother surface after 80 h of electrolysis (Figure S13). The much higher operational stability of **Foam/nanowires** is consistent with the nominal changes in morphology and the nominal mass loss (Table S1). Moreover, the same **Foam/nanowires** electrode used for this 80 h electrolysis experiment could be reused 3 weeks later without any regeneration steps to yield nearly the same performance (Figure S14). These results demonstrate how a free-standing silver foam electrode does not suffer from silver nanoparticle detachment and stability issues common to conventional GDEs, such as **GDE/control** (Table S1).

Conclusion

A key outcome of this study is that we show that aqueous bicarbonate can be electrolyzed into a single carbon-based product more effectively than any known CO_2 electrolyzer that uses an aqueous feedstock saturated with CO_2, and nearly as effectively as electrolyzers that rely on gaseous CO_2 feedstocks. We were able to achieve this by using a free-standing metallic cathodic GDE, which we found to be more effective for electrolyzing liquid bicarbonate solutions than the carbon-based GDEs widely used for CO_2RR electrolysis. While a conventional GDE containing silver nanoparticles on a carbon support yields a FE_{CO} of merely 33 ± 6% during electrolysis of bicarbonate solutions, free-standing silver foam electrodes achieve a FE_{CO} of 72 ± 3%. The electrolytic performance of this foam can be improved by increasing the ECSA (e.g., etching, coating with nanowires), or by operating at higher temperatures. Importantly, the free-standing electrodes are also far more stable than the conventional GDEs that suffer from catalyst detachment. The free-standing electrodes are also easier to

assemble, and they can be re-used without further regeneration steps. We therefore contend that this architecture provides a viable path for making CO_2 electrolysis compatible with carbon capture schemes.

Experimental procedures

Cathode Preparation

The silver foam and nickel foam were cut into desired dimensions (2 × 2 cm) with a blade and washed with acetone and water. The silver foam (0.085 g cm^{-2}) was treated with dilute nitric acid solution (25% v/v HNO_3) in a 50 ml beaker for 10 s to remove the oxide layer and increase its electrochemical surface area. The etched silver foam (0.070 g cm^{-2}) was further washed thoroughly with deionized (DI) water, followed by a rinse with 3 M $KHCO_3$. 200 µl silver nanowires solution was dispersed in 2.0 ml isopropyl alcohol (IPA) by sonication and was then hand-sprayed onto the etched silver foam substrate (silver nanowire loading: 5.90 ± 0.46 mg). The prepared electrode was stored in DI water for further use.

To fabricate traditional GDEs with silver nanoparticles **(GDE/control**), a catalyst ink was prepared by mixing 315 mg silver nanoparticles, 15 ml DI water, 15 ml IPA and 420 µl Nafion® 117 solution. The catalyst ink was then spray-coated on the carbon cloth to make multiple GDEs, and each GDE (geometric area: 4 cm^2) has silver loadings of 3.7 ± 0.1 mg cm^{-2}.

Controlled Temperature Experiments

The catholyte reservoir was placed in a water bath with increased temperatures (T_{bath}) and was allowed to reach thermal equilibrium before electrolysis. The temperature of the catholyte entering the flow cell was measured right at the inlet of the cathode flow plate (T_{inlet}), since some heat losses were expected during the transfer of liquid from the reservoir to the flow cell.

Acknowledgements

The authors would like to thank Dr. Tengfei Li and Arthur G. Fink for valuable discussions, David J. Dvorak for performing scanning electron microscopy (SEM) imaging, and Danika Wheeler for making resistance temperature detectors (RTD) for temperature measurements. The authors are grateful to Natural Resources Canada (EIP2-MAT-001), the Canadian Natural Science and Engineering Research Council (RGPIN 337345-13), Canadian Foundation for Innovation (229288), Canadian Institute for Advanced Research (BSE-BERL-162173), TOTAL American Services, Inc (an affiliate of TOTAL SA, France), and the Canada Research Chairs for financial support. This research was undertaken thanks in part to funding from the Canada First Research Excellence Fund, Quantum Materials and Future Technologies Program. SEM imaging was performed in the Centre for High-Throughput Phenogenomics at the University of British Columbia, a facility supported by the Canada Foundation for Innovation, British Columbia Knowledge Development Foundation, and the UBC Faculty of Dentistry.

Author contributions

C.P.B. supervised the project. Z.Z conceived the study and Z.Z, F.H., D.S., generated the figures. Z.Z. designed and executed the experiments. S.R. helped with electrolysis experiments. All authors contributed to the final manuscript writing.

References

1. Keith, D.W., Holmes, G., St. Angelo, D., and Heidel, K. (2018). A Process for Capturing CO2 from the Atmosphere. Joule *2*, 1573–1594.

2. Weekes, D.M., Salvatore, D.A., Reyes, A., Huang, A., and Berlinguette, C.P. (2018). Electrolytic CO_2 Reduction in a Flow Cell. Acc. Chem. Res. *51*, 910–918.

3. Salvatore, D.A., Weekes, D.M., He, J., Dettelbach, K.E., Li, Y.C., Mallouk, T.E., and Berlinguette, C.P. (2018). Electrolysis of Gaseous CO_2 to CO in a Flow Cell with a Bipolar Membrane. ACS Energy Lett. *3*, 149–154.

4. Nitopi, S., Bertheussen, E., Scott, S.B., Liu, X., Engstfeld, A.K., Horch, S., Seger, B., Stephens, I.E.L., Chan, K., Hahn, C., et al. (2019). Progress and Perspectives of Electrochemical CO2 Reduction on Copper in Aqueous Electrolyte. Chem. Rev. *119*, 7610–7672.

5. Burdyny, T., and Smith, W.A. (2019). CO2 reduction on gas-diffusion electrodes and why catalytic performance must be assessed at commercially-relevant conditions. Energy & Environmental Science *12*, 1442–1453.

6. Welch, A.J., Dunn, E., DuChene, J.S., and Atwater, H.A. (2020). Bicarbonate or Carbonate Processes for Coupling Carbon Dioxide Capture and Electrochemical Conversion. ACS Energy Letters *5*, 940–945.

7. Gao, D., Arán-Ais, R.M., Jeon, H.S., and Cuenya, B.R. (2019). Rational catalyst and electrolyte design for CO 2 electroreduction towards multicarbon products. Nature Catalysis *2*, 198–210.

8. Smith, W.A., Burdyny, T., Vermaas, D.A., and Geerlings, H. (2019). Pathways to Industrial-Scale Fuel Out of Thin Air from CO2 Electrolysis. Joule *3*, 1822–1834.

9. Butler, J.W., Jim Lim, C., and Grace, J.R. (2011). CO2 capture capacity of CaO in long series of pressure swing sorption cycles. Chemical Engineering Research and Design *89*, 1794–1804.

10. Lin, S., Kiga, T., Wang, Y., and Nakayama, K. (2011). Energy analysis of CaCO3 calcination with CO2 capture. Energy Procedia *4*, 356–361.

11. Li, T., Lees, E.W., Goldman, M., Salvatore, D.A., Weekes, D.M., and Berlinguette, C.P. (2019). Electrolytic Conversion of Bicarbonate into CO in a Flow Cell. Joule *3*, 1487–1497.

12. Li, Y.C., Lee, G., Yuan, T., Wang, Y., Nam, D.-H., Wang, Z., García de Arquer, F.P., Lum, Y., Dinh, C.-T., Voznyy, O., et al. (2019). CO2 Electroreduction from Carbonate Electrolyte. ACS Energy Lett. *4*, 1427–1431.

13. Vermaas, D.A., and Smith, W.A. (2016). Synergistic Electrochemical CO2 Reduction and Water Oxidation with a Bipolar Membrane. ACS Energy Lett. *1*, 1143–1148.

14. Li, J., Chen, G., Zhu, Y., Liang, Z., Pei, A., Wu, C.-L., Wang, H., Lee, H.R., Liu, K., Chu, S., et al. (2018). Efficient electrocatalytic CO2 reduction on a three-phase interface. Nature Catalysis *1*, 592–600.

15. Weber, A.Z., and Newman, J. (2005). Effects of Microporous Layers in Polymer Electrolyte Fuel Cells. J. Electrochem. Soc. *152*, A677–A688.

16. Kumar, S.S., and Himabindu, V. (2019). Hydrogen production by PEM water electrolysis--A review. Materials Science for Energy Technologies.

17. Dias, A.C. de B.V., and Others (2010). Chlor-alkali membrane cell process: study and characterization.

18. Xiang, C., Papadantonakis, K.M., and Lewis, N.S. (2016). Principles and implementations of electrolysis systems for water splitting. Materials Horizons *3*, 169–173.

19. Zeng, K., and Zhang, D. (2010). Recent progress in alkaline water electrolysis for hydrogen production and applications. Progress in Energy and Combustion Science *36*, 307–326.

20. Franco, F., Prior, J., Velizarov, S., and Mendes, A. (2019). A Systematic Performance History Analysis of a Chlor-Alkali Membrane Electrolyser under Industrial Operating Conditions. NATO Adv. Sci. Inst. Ser. E Appl. Sci. *9*, 284.

21. Achieved, S.E.S.C.B.E. (1985). Platinum Metals Activated Cathodes for the Chloralkali Industry. Platin. Met. Rev. *29*, 98–106.

22. Lees, E.W., Goldman, M., Fink, A.G., Dvorak, D.J., Salvatore, D.A., Zhang, Z., Loo, N.W.X., and Berlinguette, C.P. (2020). Electrodes Designed for Converting Bicarbonate into CO. ACS Energy Letters, 2165–2173.

23. Larrazábal, G.O., Strøm-Hansen, P., Heli, J.P., Zeiter, K., Therkildsen, K.T., Chorkendorff, I., and Seger, B. (2019). Analysis of Mass Flows and Membrane Cross-over in CO2 Reduction at High Current Densities in an MEA-Type Electrolyzer. ACS Appl. Mater. Interfaces *11*, 41281–41288.

24. Kutz, R.B., Chen, Q., Yang, H., Sajjad, S.D., Liu, Z., and Richard Masel, I. (2017). Sustainion Imidazolium-Functionalized Polymers for Carbon Dioxide Electrolysis. Energy Technology *5*, 929–936.

25. Ren, S., Joulié, D., Salvatore, D., Torbensen, K., Wang, M., Robert, M., and Berlinguette, C.P. (2019). Molecular electrocatalysts can mediate fast, selective CO2 reduction in a flow cell. Science *365*, 367–369.

26. Verma, S., Hamasaki, Y., Kim, C., Huang, W., Lu, S., Jhong, H.-R.M., Gewirth, A.A., Fujigaya, T., Nakashima, N., and Kenis, P.J.A. (2018). Insights into the Low Overpotential Electroreduction of CO2 to CO on a Supported Gold Catalyst in an Alkaline Flow Electrolyzer. ACS Energy Lett. *3*, 193–198.

27. Diaz, L.A., Gao, N., Adhikari, B., Lister, T.E., Dufek, E.J., and Wilson, A.D. (2018). Electrochemical production of syngas from CO2 captured in switchable polarity solvents. Green Chemistry *20*, 620–626.

28. Li, Y.C., Zhou, D., Yan, Z., Gonçalves, R.H., Salvatore, D.A., Berlinguette, C.P., and Mallouk, T.E. (2016). Electrolysis of CO2 to Syngas in Bipolar Membrane-Based Electrochemical Cells. ACS Energy Lett. *1*, 1149–1153.

29. Delacourt, C., Ridgway, P.L., Kerr, J.B., and Newman, J. (2008). Design of an Electrochemical Cell Making Syngas (CO H[sub 2]) from CO[sub 2] and H[sub 2]O Reduction at Room Temperature. Journal of The Electrochemical Society *155*, B42.

30. Dufek, E.J., Lister, T.E., Stone, S.G., and McIlwain, M.E. (2012). Operation of a Pressurized System for Continuous Reduction of CO2. J. Electrochem. Soc. *159*, F514.

31. Dutta, A., Morstein, C.E., Rahaman, M., Cedeño López, A., and Broekmann, P. (2018). Beyond Copper in CO2 Electrolysis: Effective Hydrocarbon Production on Silver-Nanofoam Catalysts. ACS Catal. *8*, 8357–8368.

32. Kottakkat, T., Klingan, K., Jiang, S., Jovanov, Z.P., Davies, V.H., El-Nagar, G.A.M., Dau, H., and Roth, C. (2019). Electrodeposited AgCu Foam Catalysts for Enhanced Reduction of CO2 to CO. ACS Appl. Mater. Interfaces *11*, 14734–14744.

33. Lu, Q., Rosen, J., Zhou, Y., Hutchings, G.S., Kimmel, Y.C., Chen, J.G., and Jiao, F. (2014). A selective and efficient electrocatalyst for carbon dioxide reduction. Nat. Commun. *5*, 3242.

34. Xi, W., Ma, R., Wang, H., Gao, Z., Zhang, W., and Zhao, Y. (2018). Ultrathin Ag Nanowires Electrode for Electrochemical Syngas Production from Carbon Dioxide. ACS Sustainable Chem. Eng. *6*, 7687–7694.

35. Back, S., Yeom, M.S., and Jung, Y. (2015). Active sites of Au and Ag nanoparticle catalysts for CO2

electroreduction to CO. ACS Catal. *5*, 5089–5096.

36. Sun, D., Xu, X., Qin, Y., Jiang, S.P., and Shao, Z. (2020). Rational design of Ag-based catalysts for the electrochemical CO2 reduction to CO: a review. ChemSusChem *13*, 39–58.

37. Weng, L.-C., Bell, A.T., and Weber, A.Z. (2018). Modeling gas-diffusion electrodes for CO2 reduction. Physical Chemistry Chemical Physics *20*, 16973–16984.

38. Kim, B., Hillman, F., Ariyoshi, M., Fujikawa, S., and Kenis, P.J.A. (2016). Effects of composition of the micro porous layer and the substrate on performance in the electrochemical reduction of CO2 to CO. J. Power Sources *312*, 192–198.

39. Feng, Y., Zheng, H., Zhu, Z., and Zu, F. (2003). The microstructure and electrical conductivity of aluminum alloy foams. Mater. Chem. Phys. *78*, 196–201.

40. Ismail, M.S., Damjanovic, T., Ingham, D.B., Pourkashanian, M., and Westwood, A. (2010). Effect of polytetrafluoroethylene-treatment and microporous layer-coating on the electrical conductivity of gas diffusion layers used in proton exchange membrane fuel cells. J. Power Sources *195*, 2700–2708.

41. Omrani, R., and Shabani, B. (2017). Gas diffusion layer modifications and treatments for improving the performance of proton exchange membrane fuel cells and electrolysers: A review. Int. J. Hydrogen Energy *42*, 28515–28536.

42. Cao, Y., Gao, Z., Jin, J., Zhou, H., Cohron, M., Zhao, H., Liu, H., and Pan, W. (2008). Synthesis Gas Production with an Adjustable H2/CO Ratio through the Coal Gasification Process: Effects of Coal Ranks And Methane Addition. Energy Fuels *22*, 1720–1730.

43. Lobaccaro, P., Singh, M.R., Clark, E.L., Kwon, Y., Bell, A.T., and Ager, J.W. (2016). Effects of temperature and gas-liquid mass transfer on the operation of small electrochemical cells for the quantitative evaluation of CO2 reduction electrocatalysts. Phys. Chem. Chem. Phys. *18*, 26777–26785.

44. Johnson, K.S. (1982). Carbon dioxide hydration and dehydration kinetics in seawater 1. Limnol. Oceanogr. *27*, 849–855.

45. Lobaccaro, P., Singh, M.R., Clark, E.L., Kwon, Y., Bell, A.T., and Ager, J.W. (2016). Effects of temperature and gas--liquid mass transfer on the operation of small electrochemical cells for the quantitative evaluation of CO 2 reduction electrocatalysts. Phys. Chem. Chem. Phys. *18*, 26777–26785.